



OPEN Interaction preferences between protein side chains and key epigenetic modifications 5-methylcytosine, 5-hydroxymethylcytosine and N⁶-methyladenine

Matea Hajnic^{1,2}, Santiago Alonso Gil¹, Anton A. Polyansky¹, Anita de Ruiter^{1,3} & Bojan Zagrovic¹✉

Covalent modifications of standard DNA/RNA nucleobases affect epigenetic regulation of gene expression by modulating interactions between nucleic acids and protein readers. We derive here the absolute binding free energies and analyze the binding modalities between key modified nucleobases 5-methylcytosine (5mC), 5-hydroxymethylcytosine (5hmC) and N⁶-methyladenine (m⁶A) and all non-prolyl/non-glycyl protein side chains using molecular dynamics simulations and umbrella sampling in both water and methanol, the latter mimicking the low dielectric environment at the dehydrated nucleic-acid/protein interfaces. We verify the derived affinities by comparing against a comprehensive set of high-resolution structures of nucleic-protein complexes involving 5mC. Our analysis identifies protein side chains that are highly tuned for detecting cytosine methylation as a function of the environment and can thus serve as microscopic readers of epigenetic marks. Conversely, we show that the relative ordering of sidechain affinities for 5hmC and m⁶A does not differ significantly from those for their precursor bases, cytosine and adenine, respectively, especially in the low dielectric environment. For those two modified bases, the effect is more nuanced and manifests itself primarily at the level of absolute changes in the binding free energy. Our results contribute towards establishing a quantitative foundation for understanding, predicting and modulating the interactions between modified nucleic acids and proteins at the atomistic level.

Modifications of standard DNA/RNA nucleobases greatly amplify the amount of information encoded in nucleic acid sequences and are associated with epigenetic regulation of gene expression and modulation of transcript stability^{1–3}. In DNA, modified nucleobases play key roles in cell differentiation, aging and disease development by either remodeling chromatin structure or affecting directly the DNA/protein interactions^{1,2,4–6}. In RNA, nucleobase modifications affect different molecular processes, including mRNA transcription, splicing, export, translation and degradation^{3,7–10}. Notably, the impact of the DNA/RNA modifications on gene expression and transcript stability has mostly been studied from the perspective of how the change in their genomic or transcriptomic patterns affects the cellular or organismic phenotype^{3,5}. However, less is known about the atomistic mechanisms behind such phenotypic changes and, in particular, how nucleobase modifications affect the interactions between the modified nucleic acids and protein readers, which detect them. In general, DNA and RNA recognition by proteins depends on different environmental, structural and dynamical determinants. Importantly, such recognition also directly depends on the intrinsic binding preferences between the individual nucleobases and amino acids in different environments¹¹. While the binding preferences between standard nucleobases and

¹Department of Structural and Computational Biology, Max Perutz Labs, University of Vienna, Campus Vienna Biocenter 5, 1030 Vienna, Austria. ²Present address: Bayer AG, Computational Life Sciences, Research & Development, Crop Science, Frankfurt, Germany. ³Present address: Institute of Molecular Modeling and Simulation, BOKU, Muthgasse 18, 1190 Vienna, Austria. ✉email: bojan.zagrovic@univie.ac.at

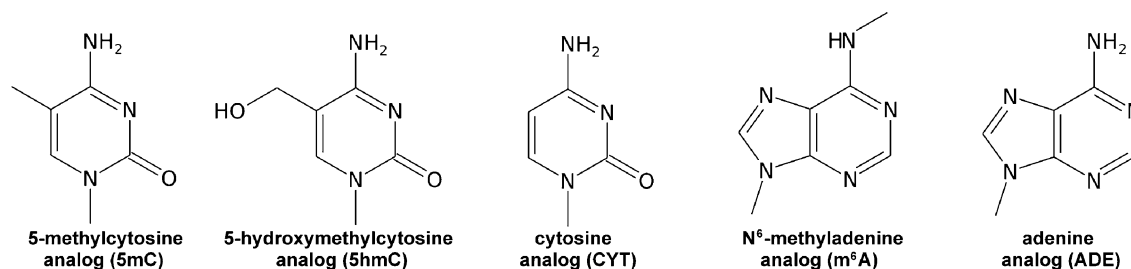


Figure 1. Chemical structures of 5mC, 5hmC, CYT, m⁶A and ADE analogs used in simulations.

amino acids have in general been well studied^{11–20}, much less is known about how these preferences change in the case of typical nucleobase modifications, with most work focusing on the overall impact of modifications on the affinities between complete nucleic acids and proteins^{21–24}.

Motivated by this, we focus here on the interaction preferences between protein side chains and three abundant and well-studied modified nucleobases with critical roles in both DNA and RNA biology: 5-methylcytosine (5mC)^{5,6,25–27}, 5-hydroxymethylcytosine (5hmC)^{25,28–31} and N⁶-methyladenine (m⁶A)^{3,32–35} (Fig. 1). Specifically, 5mC, a modified derivative of cytosine (CYT), is the most abundant modification in DNA that is introduced by different DNA- and RNA-methyltransferases^{6,10,36,37} (Fig. 1). It has been estimated that ~4% of all DNA CYTs in mammals are modified to 5mC, while in the CpG regions this fraction increases to ~80%⁵. 5mC is mostly found within promoter and enhancer regions, where its occurrence is associated with gene repression⁴. In DNA, 5mC is recognized by methyl-CpG-binding domain (MBD) proteins that bind methylated CpG regions^{37,38} and recruit different histone modifiers^{37,39,40}. Importantly, many transcription factors (TFs) are sensitive to CYT methylation in DNA⁴¹, with a caveat that trends observed in vitro do not necessarily hold in vivo⁴². Finally, in RNA, 5mC is recognized by different readers, such as ALYREF²⁷ and YBX1²⁵, which modulate RNA stability¹⁰.

In both DNA and RNA, 5mC is oxidized to another prominent modified nucleobase, 5hmC (Fig. 1), by the Ten eleven translocation (TET) enzymes^{30,31,43}. 5hmC has been found in DNA promoter and enhancer regions where its occurrence correlates positively with gene expression. The abundance of 5hmC has been estimated at 0.1% of DNA cytosines in mammalian tissues²⁸, with this fraction increasing up to 1% in the nervous system^{5,44}. Furthermore, the number of known proteins that recognize and bind 5hmC in DNA is rapidly growing to now include TET enzymes, some transcription factors, UHRF2, MBD3 and MeCP2^{5,28,30,37}. While 5mC is typically associated with the repression of transcription, its first derivative 5hmC is mostly responsible for the restoration of active transcription^{5,28,30,37}. The amounts of RNA 5hmC have been found to correlate with transcript abundance⁴⁵, but in contrast to DNA 5hmC, the nature and the functional role of readers of RNA 5hmC remain to be explored.

Finally, adenine modification m⁶A (Fig. 1) is the most frequent internal mRNA modification, with important roles in different cellular and physiological processes, ranging from splicing to translation to regulation of mRNA stability^{3,10}. m⁶A is primarily added to mRNAs via a writer complex consisting of the core N6-adenosine methyltransferase METTL3 and its adaptors⁴⁶, while its readers belong to a diverse group including YT521-B homology (YTH) domain-containing proteins, heterogeneous nuclear ribonucleoproteins, and insulin-like growth factor 2 mRNA-binding proteins^{3,8,10,46,47}. When it comes to DNA, m⁶A has been identified in different organisms at levels of up to 0.4% genomic adenines and is introduced in DNA by writers such as methyltransferase DAMT-1 in *C. elegans*^{3,32–35,48–50}. These studies have also identified demethylation enzymes (TET homologues) whose depletion is tightly correlated with m⁶A abundance^{32–34}. In mammals, m⁶A has largely been found within transposons and its occurrence has been positively correlated with their silencing and the repression of transcription from adjacent genes³³. Finally, there are a number of eraser proteins, which recognize and remove the above DNA/RNA nucleobase modifications^{3,46,51}.

While there exist hundreds of different biological relevant DNA/RNA nucleobase modifications, we focus on 5mC, 5hmC and m⁶A due to their overall abundance and biological/biomedical significance, as outlined above. Overall, our primary aim is to contribute to the fundamental understanding of the interactions between modified nucleobases and protein readers from a reductionist, physicochemical perspective. Specifically, we use atomistic molecular dynamics (MD) simulations and umbrella sampling to derive for the first time the absolute binding free energies and the associated interaction mechanisms between 5mC, 5hmC and m⁶A nucleobases and all standard, non-glycyl/non-prolyl amino-acid side chains in water and methanol. The latter is chosen as an approximation of the low-dielectric environment at nucleic-acid/protein interfaces^{12,52–54}. We compare the obtained absolute binding free energies to the corresponding binding free energies of standard nucleobases (Fig. 1) derived previously¹² and rationalize the binding mechanisms in known systems in light of the newly obtained binding affinity scales.

Materials and methods

Parameterization of modified nucleobases. Parameters for modified nucleobases were derived from those corresponding to the most similar nucleobases in the GROMOS 54a8 force field⁵⁵. Specifically, the cytosine nucleobase parameters were used as a scaffold for both 5mC and 5hmC. In the case of 5mC, the parameters for the methyl group at C5 position were taken from thymine. The hydroxymethyl group parameters of 5hmC at C5 position correspond to the parameters of the serine sidechain analog. The parameters of adenine were used for m⁶A, with the only change made for the amino group at the C6 position, where one of the hydrogen atoms

was replaced with the parameters taken from the peptide bond. The N⁶-methyl group was set in the plane of the base and pointing in the direction of the Watson–Crick edge i.e. m⁶A was simulated as a free (not base-paired) base. In addition, the methyl group at position N9 was added to all modified nucleobases at the site of sugar attachment. Side chains were parameterized to match the corresponding amino acids with the backbone atoms replaced by a single H-atom attached to C β to change it from CH₂ to CH₃ i.e. backbone was fully removed. As the applied force field uses a united-atom formalism, this effectively just meant that C β was treated as a single interacting particle with parameters of the methyl group CH₃.

Molecular dynamics (MD) simulations. MD simulations with umbrella sampling were used to derive the absolute binding free energies of all 18 natural amino-acid side chains (all except Gly and Pro) and 5mC, 5hmC or m⁶A in both water and methanol. In each simulation setup, a single modified nucleobase and a single amino-acid side chain were placed in a cubic simulation box with centers of geometries 2 nm apart and immersed in one of the two solvents. All simulations were carried out using the GROMACS 5.0 simulation package^{56,57} and united-atom GROMOS 54a8 force field⁵⁵ with a 2 fs integration step. The SPC water model^{58,59} was used in water simulations with anywhere between 3074 to 3878 water molecules per box (with the length of a cubic box between 4.5 and 4.9 nm). Box sizes remained the same in methanol simulations, but the number of solvent molecules changed to 1366–1765, depending on the system. Ionizable protein sidechains were set to correspond to a pH of 7. Histidine residue was simulated in its charged (His_H) and both neutral forms (His_A, His_B). All bonds were constrained using LINCS⁶⁰, while non-bonded interactions within a 0.8 nm range were calculated based on a pairlist that was updated every 5 steps. The interactions between 0.8 and 1.4 nm were calculated only with every pairlist update and were kept constant otherwise. Interactions beyond 1.4 nm were treated via a reaction-field contribution with a dielectric permittivity of 61 for SPC water⁵⁹ and 18.6 for methanol⁶¹. The temperature and the pressure were kept at 298 K using the Berendsen thermostat⁵⁸ ($\tau_T = 0.1$ ps) and 1 atm using the Berendsen barostat ($\tau_p = 0.5$ ps, compressibility = 4.5×10^{-5} bar⁻¹ in water^{58,62} or 1.25×10^{-4} bar⁻¹ in methanol^{63,64}), respectively.

Steepest descent algorithm with 25,000 steps was used for energy minimization. The equilibration was performed in six independent steps. In the first step, position restraints (with a force constant of 2.5×10^4 kJ mol⁻¹) were applied to solute molecules, with the initial velocities drawn from the Maxwell–Boltzmann distribution at 50 K. In the next four equilibration steps, the temperature was raised by 50 K and the force constant of the position restraints lowered by a factor of 10 at each step. In the last equilibration step, the temperature was set to 298 K, while position restraints were switched-off and center-of-mass-translation was removed every 1000 steps. The first four equilibration steps were simulated for 20 ps each, while the last step took 40 ps. All equilibration steps were performed in the NPT ensemble.

Umbrella sampling. The absolute binding free energies of amino-acid sidechain/modified nucleobase pairs were derived from potentials of mean force (PMFs) using the methodology previously described in de Ruiter et al.¹² Here, the PMFs were constructed using the distance between the centers of geometry of a modified nucleobase and an amino-acid side chain as the reaction coordinate. To enhance the sampling along the reaction coordinate, umbrella sampling with a force constant of 500 kJ mol⁻¹ nm⁻² was used. The restraining distances ranged from 0.4 to 1.9 nm and were changed in steps of 0.1 nm. At each step, an equilibration of 100 ps preceded a production run of 10 ns. To test for convergence, the production runs were split into two 5-ns long segments, and the PMFs and the binding free energies calculated for each. If the difference in $\Delta G_{\text{binding}}$ between the two segments exceeded 1.5 kJ/mol, the production runs for all distances were prolonged for additional 10 ns until this criterion was met.

Analysis of amino-acid enrichment at known 5mC/CYT interfaces. A comprehensive set containing all available X-ray structures of unique nucleic-acid/protein complexes in which CYT and 5mC moieties interact directly with the same protein was obtained from the PDB. The average resolution of the 101 X-ray structures in the set (PDB codes given in the Supplementary Information) was 2.2 ± 0.4 Å, with the lowest resolution being 3.2 Å. Enrichment E was defined as the ratio of the total relative surface area corresponding to a given amino acid at the interface with a given nucleobase and the total relative surface area occupied by the amino acid on the whole surface. A proxy of the relative binding free energy of a given amino acid with CYT and 5mC was estimated as the negative natural logarithm of the ratio between the average enrichment of residues in direct van-der-Waals contact with 5mC or CYT i.e. $-\ln(E(5mC)/E(CYT))$, and compared with the Factor 1 hydrophobicity scale⁶⁵ and $\Delta\Delta G_{\text{methanol}}$ values. For Factor 1 comparison, amino acids were additionally grouped by their physicochemical properties as follows: apolar (Ala, Cys, Ile, Leu, Met, Val), aromatic (Phe, Trp, Tyr, His), OH-containing (Ser, Thr), amide-containing (Asn, Gln), positively charged (Arg, Lys), negatively charged (Asp, Glu), while Gly and Pro were treated individually and were not grouped with other amino acids for this analysis.

Results

Protein sidechain binding free energies of 5mC and 5hmC. The potentials of mean force (PMFs) derived from MD simulations suggest that in water 5mC interacts most strongly with the aromatic side chains of Trp, Tyr and Phe, with the corresponding absolute $\Delta G_{5mC(\text{water})}$ of -4.3 kJ/mol, -3.9 kJ/mol and -3.0 kJ/mol, respectively (Fig. 2A left, Table 1 and Fig. S1). The same trend is also observed for 5hmC in water, with the slightly more favorable $\Delta G_{5hmC(\text{water})}$ values of -4.8 kJ/mol for Trp, -4.2 kJ/mol for Tyr and -3.5 kJ/mol for Phe (Fig. 2a right, Table 1 and Fig. S2). On the other hand, neither CYT derivative exhibits any preference for the negatively charged side chains in water (Figs. 2a, S1 and S2, Table 1). Importantly, the amino-acid binding free energies of 5mC and 5hmC correlate with each other with a Spearman correlation coefficient $\rho = 0.91$ and

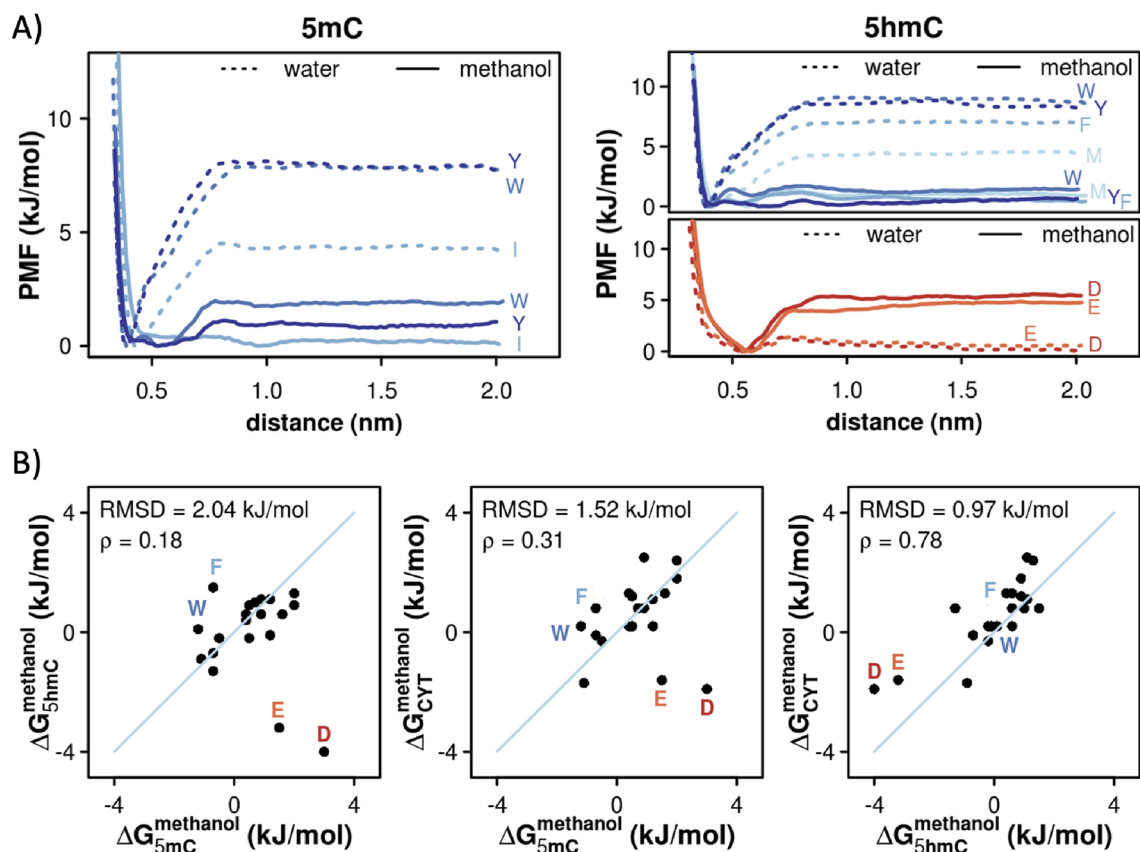


Figure 2. Absolute binding free energies of protein side chains for 5mC and 5hmC. (a) PMF curves derived for protein side chains whose affinities for 5mC (left panel) and 5hmC (right panels) change significantly (> 3 kJ/mol) depending on the surrounding solvent. (b) A comparison between sidechain affinity scales in methanol for: 5mC and 5hmC (left panel), 5mC and CYT¹² (middle panel) and 5hmC and CYT (right panel) with the corresponding Spearman correlation coefficients and RMSD values. Side chains that deviate the most in the affinities for the two nucleobases being compared are labeled in color.

	water								
	CYT	5mC	5hmC	ADE	m ⁶ A	5mC-CYT	5hmC-CYT	m ⁶ A-ADE	
Ala	0.9	0.4	-0.5	0.2	0.6	-0.5	-1.4	0.4	
Arg	-1.1	-1.3	-2	-0.8	-1.7	-0.2	-0.9	-0.9	
Asn	-0.7	-0.9	-1.4	-1	-2.4	-0.2	-0.7	-1.4	
Asp	2.4	3.9	1.3	0.5	1.9	1.5	-1.1	1.4	
Cys	-0.2	-1.2	-0.7	-1.2	-0.7	-1	-0.5	0.5	
Gln	-0.5	-1	-1.4	-2	-1.9	-0.5	-0.9	0.1	
Glu	1.6	3.3	0.6	2	2.3	1.7	-1	0.3	
HisA	-0.9	-2	-1.7	-1.8	-2.8	-1.1	-0.8	-1	
HisB	-0.2	-1.1	-1.1	-1.2	-1.8	-0.9	-0.9	-0.6	
HisH	0	-0.8	-0.8	-0.7	-0.4	-0.8	-0.8	0.3	
Ile	-1.9	-2.1	-2.2	-2.8	-1.8	-0.2	-0.3	1	
Leu	-1.9	-1.9	-2	-2	-2	0	-0.1	0	
Lys	1.4	-0.2	-0.4	0.9	-0.7	-1.6	-1.8	-1.6	
Met	-1.4	-2.4	-2.5	-2.5	-2.9	-1	-1.1	-0.4	
Phe	-2.7	-3	-3.5	-3.3	-3.4	-0.3	-0.8	-0.1	
Ser	1.1	-0.1	1.1	0.3	0.9	-1.2	0	0.6	
Thr	0.6	-1	-0.9	-0.5	-0.5	-1.6	-1.5	0	
Trp	-3.6	-4.3	-4.8	-3.8	-5.2	-0.7	-1.2	-1.4	
Tyr	-3.3	-3.9	-4.2	-3.9	-5.1	-0.6	-0.9	-1.2	
Val	-1.2	-1.6	-1.4	-1.5	-2.1	-0.4	-0.2	-0.6	

Table 1. $\Delta G_{binding}$ in water between protein side chains and CYT, 5mC, 5hmC, ADE or m⁶A, together with $\Delta\Delta G_{binding}$ of modified nucleobases with respect to their standard counterparts. The values for CYT and ADE were taken from de Ruiter et al.¹². All values are given in kJ/mol.

	methanol							
	CYT	5mC	5hmC	ADE	m ⁶ A	5mC-CYT	5hmC-CYT	m ⁶ A-ADE
Ala	2.5	0.9	1.1	1.2	1.8	-1.6	-1.4	0.6
Arg	0.8	-0.7	-1.3	2.8	2	-1.5	-2.1	-0.8
Asn	1.1	1.2	1.1	0.5	1	0.1	0	0.5
Asp	-1.9	3	-4	1.8	2.9	4.9	-2.1	1.1
Cys	0.8	0.9	0.6	0.4	0.4	0.1	-0.2	0
Gln	0.8	0.7	1	0.8	1.1	-0.1	0.2	0.3
Glu	-1.6	1.5	-3.2	2.3	3.2	3.1	-1.6	0.9
HisA	0.2	0.5	-0.2	0.2	0.5	0.3	-0.4	0.3
HisB	0.2	1.2	-0.1	0.5	0.5	1	-0.3	0
HisH	-1.7	-1.1	-0.9	0.8	2.1	0.6	0.8	1.3
Ile	1.3	1.6	0.6	0.7	0.2	0.3	-0.7	-0.5
Leu	0.2	0.4	0.6	0.1	0.8	0.2	0.4	0.7
Lys	-0.1	-0.7	-0.7	3	2.8	-0.6	-0.6	-0.2
Met	1.2	0.5	0.9	-0.3	-0.3	-0.7	-0.3	0
Phe	0.8	-0.7	1.5	-0.7	-0.3	-1.5	0.7	0.4
Ser	2.4	2	1.3	1.1	2.1	-0.4	-1.1	1
Thr	1.8	2	0.9	0.4	1.4	0.2	-0.9	1
Trp	0.2	-1.2	0.1	-1.2	-0.5	-1.4	-0.1	0.7
Tyr	-0.3	-0.5	-0.2	0.1	-0.2	-0.2	0.1	-0.3
Val	1.3	0.4	0.4	0.1	0.7	-0.9	-0.9	0.6

kJ/mol

Table 2. $\Delta G_{\text{binding}}$ in methanol between protein side chains and CYT, 5mC, 5hmC, ADE or m⁶A, together with $\Delta\Delta G_{\text{binding}}$ of modified nucleobases with respect to their standard counterparts. The values for CYT and ADE were taken from de Ruiter et al.¹². All values are given in kJ/mol.

a root-mean square deviation (RMSD) over all studied amino acids of 0.96 kJ/mol. Finally, the amino-acid free energies of both 5mC and 5hmC in water correlate closely with the corresponding binding free energies of their precursor nucleobase CYT¹² (Table 1) with Spearman $\rho_{5\text{mC-C}}(\text{water}) = 0.95$ and $\rho_{5\text{hmC-C}}(\text{water}) = 0.97$ and RMSDs of 0.95 and 0.96 kJ/mol, respectively.

The PMFs derived in methanol, a low-dielectric solvent meant to model the largely dehydrated RNA–protein interfaces, lead to significantly less favorable binding free energies of 5mC for most side chains as compared to in water (Tables 1 and 2, Fig. S1). Indeed, the biggest change is observed for Ile, Tyr and Trp where the binding free energies become significantly less favorable ($\Delta\Delta G_{5\text{mC}}(\text{methanol-water}) > 3$ kJ/mol). A similar behavior is observed for 5hmC, especially for Phe, Trp, Tyr and Met (Tables 1 and 2, Fig. S2). On the other hand, the binding free energies between 5hmC and the negatively charged Asp and Glu become significantly more favorable in methanol as compared to water ($\Delta\Delta G_{5\text{hmC}}(\text{methanol-water}) < -3.8$ kJ/mol, Tables 1 and 2). Unlike in water, the protein sidechain affinities of 5mC and 5hmC in methanol correlate with each other only weakly ($\rho_{5\text{mC-5hmC}}(\text{methanol}) = 0.18$ and RMSD = 2.04 kJ/mol) with the biggest difference seen for Asp and Glu and, to a lesser degree, Phe and Trp (Fig. 2b, left), while the binding free energies of 5mC in methanol significantly diverge from those of CYT ($\rho_{5\text{mC-CYT}}(\text{methanol}) = 0.31$, RMSD_{5mC-CYT}(methanol) = 1.52 kJ/mol), the binding free energies of 5hmC in methanol are significantly more similar to those of CYT ($\rho_{5\text{hmC-CYT}}(\text{methanol}) = 0.78$, RMSD_{5hmC-CYT}(methanol) = 0.97 kJ/mol) (Fig. 2b, middle and right). The latter similarity stems primarily from the fact that in methanol both CYT and 5hmC interact favorably with the negatively charged side chains and unfavorably with the aromatic ones (Table 2), while with 5mC the situation is reversed. Finally, the binding free energies for the positively charged Arg and Lys side chains are the only ones where the affinities of 5hmC are more similar to 5mC than to its precursor nucleobase CYT: namely, both modified nucleobases show favorable affinities for these two side chains (Table 2).

Protein sidechain binding free energies of m⁶A. In water, m⁶A shows the strongest preference for aromatic side chains, with $\Delta G_{\text{m}^6\text{A}}(\text{water})$ of -5.2 kJ/mol for Trp, -5.1 kJ/mol for Tyr and -3.4 kJ/mol for Phe (Fig. 3a left panel, Table 1 and Fig. S3). Favorable interactions, albeit weaker, are also observed with other polar and non-polar protein side chains, while the unfavorable binding free energies are seen for the negatively charged ones. The same trend was also observed in a related study for ADE (Table 1) (24). In fact, the protein sidechain binding free energies of m⁶A and ADE are closely related ($\rho_{\text{m}^6\text{A-ADE}}(\text{water}) = 0.89$ and RMSD_{m⁶A-ADE}(water) = 0.85 kJ/mol), with m⁶A showing slightly more favorable interactions for aromatic and positively charged residues (Table 1). On the other hand, m⁶A exhibits almost no favorable interactions with any protein side chains in methanol: for example, the binding free energy of -0.5 kJ/mol for Trp is the most favorable one of the set (Table 1, Figs. 3a and S3b). The m⁶A binding free energies derived in methanol correlate closely with those in water ($\rho_{\text{m}^6\text{A}}(\text{methanol-water}) = 0.85$), but with a significant decrease in the binding free energies for the latter across the board (RMSD_{m⁶A}(methanol-water) = 2.83 kJ/mol) (Table 1 and Fig. 3b left panel). Finally, in contrast to the situation with 5mC and CYT, the m⁶A affinities in methanol are closely related to those of ADE¹² ($\rho_{\text{m}^6\text{A-ADE}}(\text{methanol}) = 0.87$ and RMSD_{m⁶A-ADE}(methanol) = 0.67 kJ/mol) (Fig. 3b right panel, Table 2).

Convergence analysis. As seen above, the difference in the binding free energies of protein sidechains for modified and standard nucleobases is in some cases lower than 1.5 kJ/mol, the value chosen as the limit

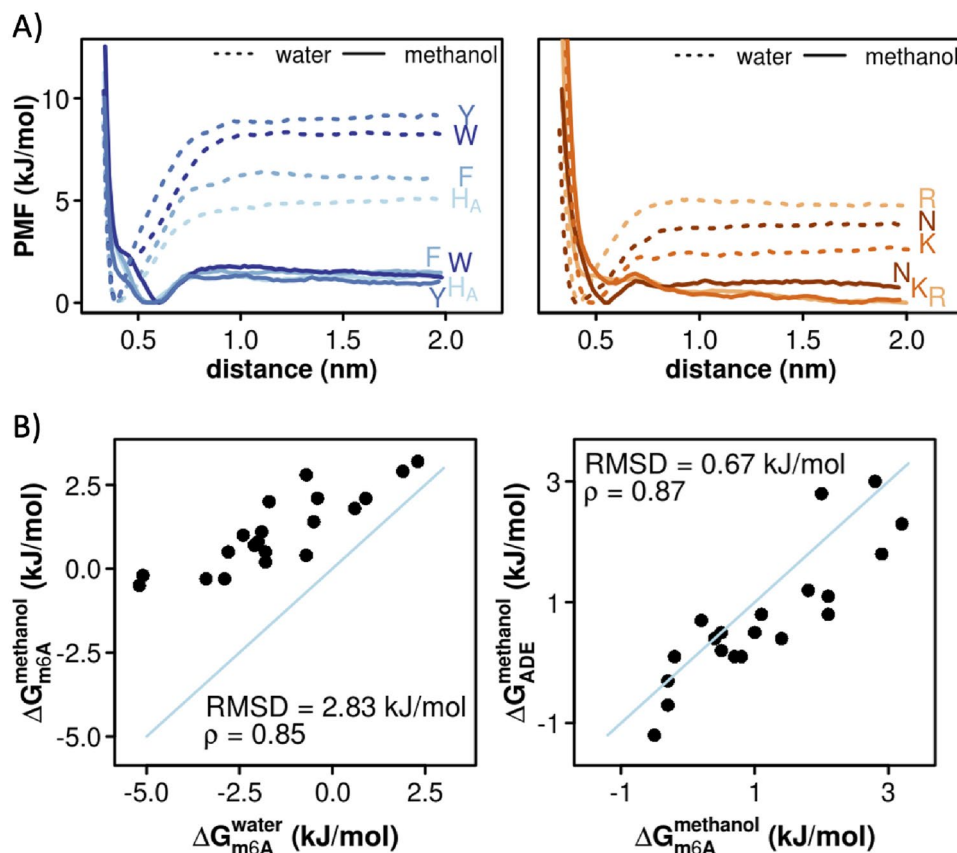


Figure 3. Absolute binding free energies of protein side chains for m⁶A. (a) PMF curves derived for protein side chains whose affinities for m⁶A change significantly (> 3.4 kJ/mol) depending on the surrounding solvent. In the left panel, affinities of aromatic side chains for m⁶A get less favorable with a decrease in the dielectric constant of the surrounding environment (from water to methanol). In the right panel, the same trend is depicted, but for polar and positively charged side chains. (b) A comparison between m⁶A sidechain affinities derived in water and methanol (left panel) and sidechain affinities for m⁶A and ADE¹² derived in methanol with the corresponding Spearman correlation coefficients and RMSD values.

for the convergence of our simulations (see Methods for details). To analyze the reproducibility of our results, we have derived the absolute binding free energies of Asp, Glu, Tyr and Trp for 5mC, 5hmC and m6A in water and methanol using 5 independent simulations for each pair, starting with different initial velocities. The largest standard deviations (SDs) in ΔG s over the five replicas were seen in the case of Asp and Glu affinities for 5mC ($SD_{Asp} = 0.55$ kJ/mol; $SD_{Glu} = 0.80$ kJ/mol) and 5hmC ($SD_{Asp} = 0.73$ kJ/mol; $SD_{Glu} = 0.92$ kJ/mol) derived in methanol (Fig. 4). Regarding m⁶A affinities, the only significant discrepancy was observed for Glu in water ($SD_{Glu} = 0.96$ kJ/mol). In all other cases, the SDs are equal or below the 0.58 kJ/mol. Overall, this analysis suggests that our simulations exhibit reasonable convergence to within an uncertainty window of 1 kJ/mol.

Dominance of π -based interactions in water. Stacking interactions between modified nucleobases and planar π -rings in amino acids represent some of the most dominant interaction modes observed in water, mirroring what was seen with unmodified bases before¹². For example, such interactions are present for 50% of time or more at the PMF minima of all three modified nucleobases and all the relevant amino acids (Arg, His_A, His_B, Phe, Trp and Tyr) except His_H, where this percentage drops to 20% (Table S1). The fact that the PMF minima in methanol are typically located at a larger distance as compared to water is reflected in the fact that the stacking interactions are destabilized in the former, with approximately an order of magnitude lower relative frequencies seen across the board (Table S1). This is fully analogous to the situation with unmodified precursor bases ADE and CYT, as shown before¹². Interestingly, in the case of 5hmC interacting with Phe, Trp or Tyr, the π - π stacking remains the dominant mode of interaction also in methanol, with the relative frequencies exceeding 50% in all three cases (Table S1). We have also analyzed the cation- π and anion- π interactions in our simulations. While in the case of m6A such interactions do not contribute significantly in the case of m6A (Table S2), they are detected in a significant fraction of simulation snapshots at the PMF minima in the case of 5mC and especially 5hmC (Table S2). For example, anion- π interactions are present in 46% of all snapshots at the PMF minimum in the case of 5hmC/Asp simulations in methanol. In agreement with the lower dielectric constant of methanol as compared to water, both cation/ π and anion/ π interactions tend to occur more frequently in methanol simulations (Table S2).

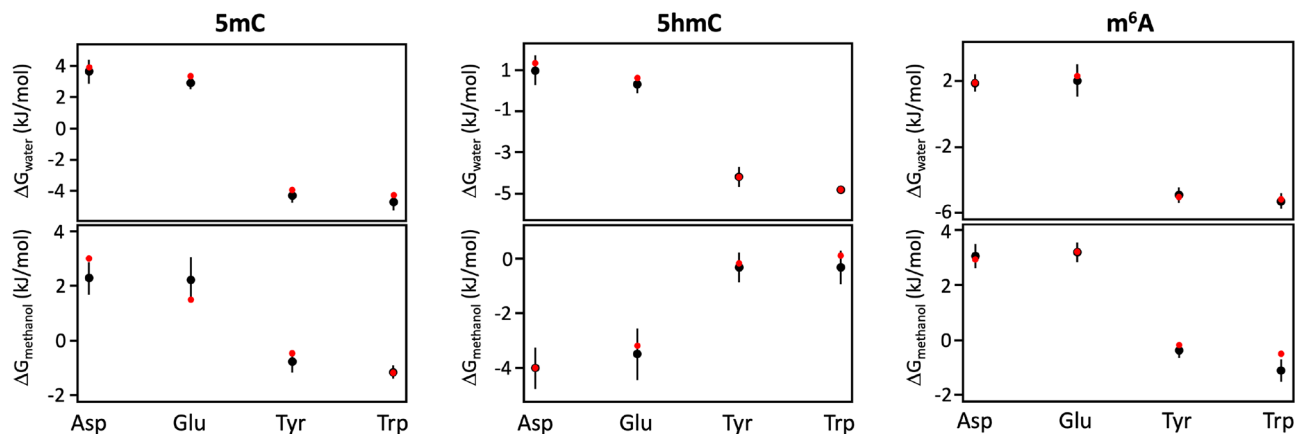


Figure 4. Convergence analysis. Means and standard deviations of $\Delta G_{\text{binding}}$ of select protein side chains (Asp, Glu, Tyr, Trp) for (a) 5mC, (b) 5hmC and (c) m⁶A, derived from 5 independent simulation runs in water and methanol. Red dots represent the values of $\Delta G_{\text{binding}}$ reported in Tables 1 and 2.

Hydrogen bonds with nucleobase ring edges represent a significant interaction mode in modified bases. Protein recognition of nucleobases in dsDNA or folded RNA occurs often with nucleobases being significantly more spatially restricted than in our umbrella simulations. Most importantly, the nucleobase ring planes may be inaccessible in such situations, shifting the emphasis on the recognition of ring edge patterns. In agreement with this, our simulations show strong evidence of hydrogen bonding with groups on the nucleobase ring that are accessible even in the context of dsDNA or folded RNA. Most prevalent H-bonds are seen between charged (Asp, Glu) or polar sidechains (Asn, Gln, His_A, His_B, Ser, Thr) and the hydroxyl group on the C5 atom and the N4 amino group of 5hmC in both water and methanol (Table S1). In addition, H-bonds are also observed between polar sidechains and the O2 group of 5hmC in methanol. A similar H-bonding pattern involving the nucleobase N4 amino group and O2 is also seen for 5mC and polar (Asn, Gln, His_A, His_B, Ser, Thr) and charged (His_H, Lys, Arg) sidechains (Table S1). We do not observe any significant interactions between sidechains and the N3 group of 5mC and 5hmC, which is inaccessible in dsDNA or folded RNA (Table S1). Finally, in the case of m⁶A, the only H-bonds that are present more than 10% of simulation time are seen between N6 amino group of the nucleobase and Asn and His_A in methanol simulations (Table S1).

5mC binding free energies modulate site-specific interactions in nucleic-acid/protein complexes. Of the three modifications studied here, the interactions of 5mC with proteins have over the years been characterized best from the structural perspective. As an illustrative example, we visualize in Fig. 5a the 3D structure of a DNA fragment in complex with the human bZIP hC/EBP β (PDB ID: 6MG3), a transcription factor (TF) which was shown to preferentially recognize 5mC-containing DNA regions⁶⁶. The family of basic region:leucine zipper (bZIP) DNA-binding proteins contains some of the most widely studied and best characterized TFs, which recognize related, but different palindromic DNA sequences as homodimers or heterodimers⁶⁷. In Fig. 5a, we highlight the hC/EBP β residues at the DNA interface, which exhibit a significant difference in their binding free energy with 5mC and CYT as derived in our methanol simulations. Our analysis shows that the residues which strongly prefer 5mC over CYT concentrate heavily at the interface between the TF and DNA, while those which prefer CYT are depleted at the interface and are enriched in the leucine zipper region of the TF (Fig. 5a). For example, Arg is heavily enriched at the interface and also exhibits one of the highest preferences for 5mC over CYT in methanol ($\Delta\Delta G_{5\text{mC-CYT}}^{\text{(methanol)}} = -1.5$ kJ/mol, Table 2). Even more significantly, the depicted variant of bZIP hC/EBP β was optimized for 5mC binding by a V285A mutation at the DNA interface and, indeed, Ala is the residue with the highest preference for 5mC over CYT in our simulations ($\Delta\Delta G_{5\text{mC-CYT}}^{\text{(methanol)}} = -1.6$ kJ/mol, Table 2)⁶⁶.

While suggestive, the bZIP hC/EBP β example is clearly an isolated case. In order to probe the general applicability of the derived scales to studying the process of detecting 5mC signals in nucleic acids, we have analyzed a comprehensive set of 101 high-resolution X-ray structures of nucleic-acid/protein complexes where CYT and 5mC are seen to interact with the same protein, revealing several notable trends. First, the preference for 5mC over CYT at nucleic-acid/protein interfaces correlates with amino-acid hydrophobicity: the more hydrophobic a given residue is, the more likely it is to be found in the vicinity of 5mC as opposed to CYT (Fig. 5b,c) and vice versa. Specifically, the statistical free-energy proxy for the relative affinity of protein residues for 5mC over CYT as derived from PDB structures correlates with the Factor 1 consensus amino-acid hydrophobicity scale⁶⁵ with a squared Pearson correlation coefficient $R^2 = 0.27$ (p-value = 0.016, Fig. 5b). This correlation also significantly increases if one groups amino acids according to their chemical properties ($R^2 = 0.58$, p-value = 0.004, Fig. 5c), but one should note that the data points in this case are associated with significant error bars and thus provide a mostly qualitative indication of proportionality only. What is more, the general trend when it comes to amino-acid enrichment at nucleic-acid/protein interfaces is consistent with the respective relative binding free energies (Fig. 5d). Specifically, all four residues with $\Delta\Delta G_{5\text{mC-CYT}}^{\text{(methanol)}} < -1$ kJ/mol i.e. those which exhibit a significant preference for 5mC in a low-dielectric environment (Trp, Ala, Phe, Arg), are in PDB structures also

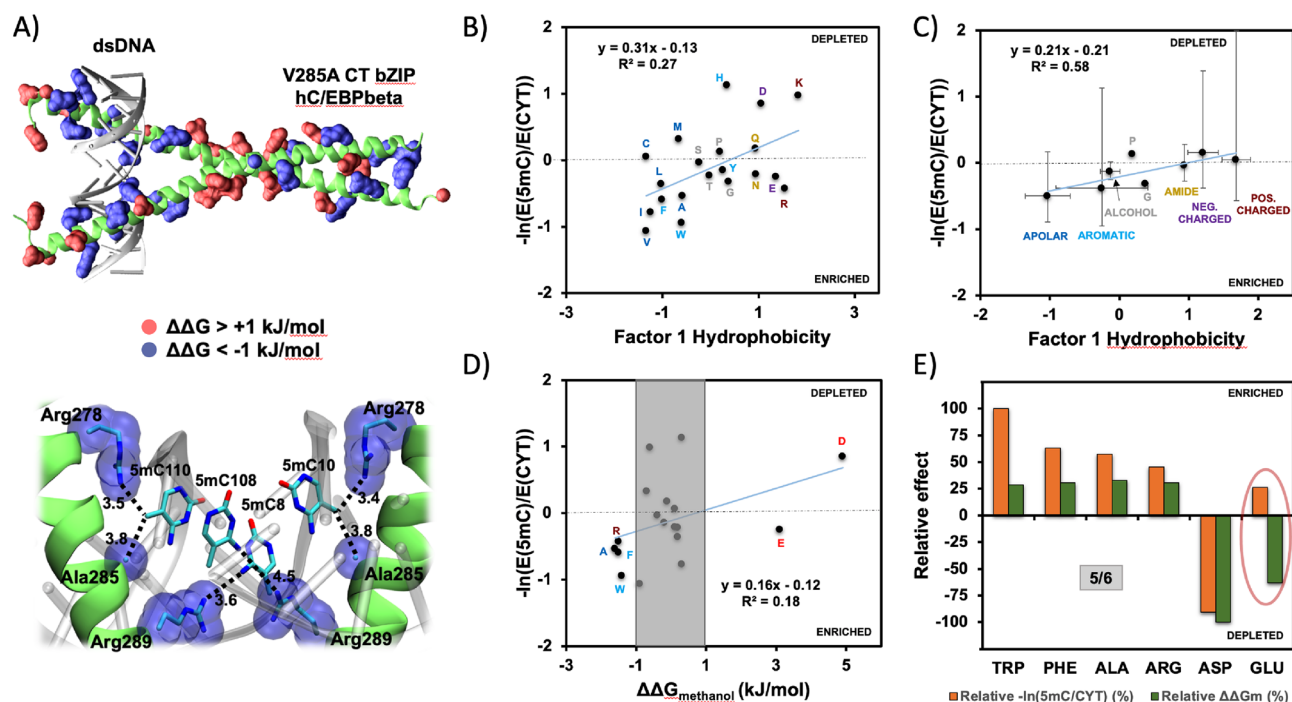


Figure 5. 5mC sidechain binding free energies guide site-specific nucleic-acid/protein interactions. (a) Structure of bZIP hC/EBP β in complex with DNA. The residues with the highest preference for 5mC over CYT in our methanol simulations are colored in blue, while the residues with the highest preference for CYT over 5mC are colored in red. (b) Correlation between hydrophobicities of amino acids as captured by Factor 1 scale⁶⁵ and their relative preference for 5mC over CYT as derived from high-resolution structures of nucleic-acid/protein complexes (Pearson $R^2 = 0.27$, p-value = 0.016). (c) Same as in (b), but with amino acids grouped according to their physicochemical properties (Pearson $R^2 = 0.58$, p-value = 0.004). (d) Comparison between $\Delta\Delta G_{5mC-CYT}(\text{methanol})$ for different protein sidechains and their relative preference for 5mC over CYT as derived from structural analysis (Pearson $R^2 = 0.18$, p-value = 0.33). (e) $\Delta\Delta G_{5mC-CYT}(\text{methanol})$ values and the relative preferences for 5mC over CYT as derived from structural analysis for residues with the highest relative preference for either 5mC (Trp, Phe, Ala, Arg) or CYT (Asp, Glu) in methanol simulations.

significantly enriched in the vicinity of 5mC as opposed to CYT (Fig. 5d,e). Also, the amino acid with the highest preference for CYT over 5mC in our methanol calculations, Asp, is significantly enriched in the vicinity of CYT as opposed to 5mC (Fig. 5d,e). In fact, of all the residues with a significant difference in binding ΔG with 5mC and CYT in a low-dielectric environment i.e. where $|\Delta\Delta G_{5mC-CYT}(\text{methanol})| > 1$ kJ/mol (points outside of the gray area in Fig. 5d), only Glu goes against the trend predicted by $\Delta\Delta G_{5mC-CYT}(\text{methanol})$. Namely, in PDB structures Glu is weakly enriched in the vicinity of 5mC as compared to CYT, although its binding free energy for CYT in methanol is more favorable by 3.1 kJ/mol (Fig. 5d,e, Table 2).

Discussion

We have provided a detailed analysis of the absolute binding free energies between standard protein side chains and three important modified nucleobases in DNA/RNA (5mC, 5hmC and m⁶A). A comparison with the corresponding free energies of standard nucleobases derived previously¹² suggests that select protein side are highly sensitive to nucleobase modifications. This effect is particularly pronounced for CYT and its modified derivative 5mC, where we observe a potentially relevant trend in the affinities derived in the low-dielectric environment especially for charged and, aromatic side chains (Fig. 2b). Thus, the presence of the negatively charged Asp and Glu at the interface strongly favors interactions with CYT, while the presence of positively charged Lys and Arg as well as aromatics favors interactions with 5mC. On the other hand, the protein side chain affinities of 5hmC resemble much more those of CYT than those of its precursor 5mC (Fig. 2b). This is especially relevant as 5hmC corresponds to the first intermediate in the active de-methylation process of 5mC performed by TET enzymes. When analyzed from a reductionist, physicochemical perspective, the CYT modification cycle could thus be seen as a two-step process, whereby the first modification of CYT to 5mC changes significantly the physicochemical properties of the original nucleobase, while the second step (5mC to 5hmC) almost completely restores the original physicochemical properties of CYT when it comes to interactions with protein side chains. Finally, it should be emphasized that both 5mC and 5hmC also affect the local flexibility of the nucleic acid in question as shown using single-molecule cyclization assays, together with molecular dynamics simulations⁶⁸. The study showed that 5mC has potential to reduce the flexibility of DNA, while 5hmC appears to enhance it, which was then further linked to the nucleosome mechanical stability with the final effect on the regulation of gene expression⁶⁸.

In contrast to CYT methylation, we do not observe a significant difference between protein sidechain affinities of ADE and its modified derivative m⁶A when it comes to the relative ordering of binding affinities (Fig. 3b). Rather, the mechanism through which m⁶A affects the interaction mode with proteins may rely more on local structural changes of DNA or RNA^{46,69–71}. The methyl group of m⁶A is positioned at the border of Watson–Crick and Hoogsteen edges, which could directly influence the base-pairing with the nucleobase from the complementary strand and lead to a local structural distortion^{46,69–71}. This could then be specifically differentiated from ADE by protein readers as already shown in the case of RNA^{8,72}. Therefore, our results suggest that the action of the m⁶A as an epigenetic marker may primarily be based on the structural effect it exerts and likely not on the difference in the physicochemical properties when compared to its chemically modified variant. This is in contrast with ADE deamination, which results in hypoxanthine (inosine base) and significantly affects interaction preferences with protein side chains⁵³. These caveats notwithstanding, it should be observed that even though the relative ordering of sidechain binding affinities does not significantly change upon ADE methylation, the $\Delta\Delta G$ values are still not all equal to 0. In other words, different residues still react differently to adenine methylation, a property that could in principle be used for modulating the activity of reader proteins.

In the present study, methanol was used to mimic the lower dielectric constant ϵ at DNA/RNA–protein interfaces. The exact value of the dielectric constant at such partially dehydrated interfaces is a local, system-specific property. For example, Alexov and coworkers have used a Gaussian dielectric model to show that the dielectric constant at DNA/RNA–protein interfaces covers a wide range going from that in protein interior to that of bulk water, depending on the exact distance between interacting atoms⁷³. In particular, they showed that the average value of ϵ tends to be between 20 and 40 for distances between nucleic acid and protein surfaces between 1 and 2 Å (DNA) or 2.5 Å and 3.5 Å (RNA). While no model solvent can capture the full complexity of realistic nucleic-acid/protein interfaces, the usage of methanol in our study enables the analysis of the effects of the medium-range values of the dielectric constant in a controlled, reductionist manner, in addition to the advantages of methanol as being an experimentally tractable solvent. Moreover, having the binding free energies between nucleobases and amino-acid side chains at two fixed points of ϵ i.e. in methanol and in water, enables one to also estimate the corresponding binding free energies at all intermediate values of ϵ between the two limits, as demonstrated before⁵⁴. Finally, it should be emphasized that the dielectric constant of the Gromos methanol model used in our study is 18.6, which is lower than its experimental value of 33⁶², but may actually be more relevant⁶¹.

We have illustrated the discriminatory power of the presently derived sidechain affinities for CYT and 5mC on the existing high-resolution structures of nucleic-acid/protein complexes (Fig. 5). We could show that the general trends in relative binding free energies determined herein largely mirror the amino-acid enrichment and depletion at the CYT and 5mC binding sites. This suggests that, at least in part, the interaction specificity between protein readers of 5mC could reside in the differences in the intrinsic affinities of protein residues for CYT and its methylated counterpart. As our results further show, these differences also depend to a degree on the dielectric properties of the local environment (Tables 1 and 2). Finally, the example of the complex between the bZIP hC/EBP β TF and DNA illustrates a wider point that TFs not only exhibit localized hot spots that bind the modified base, but rather that their entire binding interface with DNA may contribute to the final recognition of the binding site (Fig. 5a). Indeed, the trend in the hC/EBP β preference for 5mC suggests that the whole interface of TFs could be used to superficially scan for the methylation status of the DNA, leading ultimately to the site-specific binding of the methylated nucleobase. However, it should be strongly emphasized that the binding of nucleic acids and proteins, in addition to intrinsic nucleobase/amino-acid affinities, also depends on various factors, e.g. primary sequences⁷⁴, 2D and 3D structures of nucleic-acid and protein binding sites⁷⁵, cofactors⁷⁶ and chromatin accessibility⁷⁷. A clear evidence that other factors, such as steric hindrance, are also at play is given by the fact that hC/EBP β does not interact preferentially with 5hmC-containing DNA⁶⁶, although our low-dielectric scales indicate that in particular Arg residues, which feature strongly at the DNA–protein interface, should prefer 5hmC over CYT (Table 2). Finally, it should be noted that experimental crystal structures of nucleic acids are sometimes unmodified or not completely modified even in cases where modifications are expected to be detected, a fact which could skew the statistics of the relative abundancies of modified and unmodified nucleobases in our analysis.

It is our hope that this systematic study of interaction modes between three widespread modified DNA nucleobases and protein side chains with the corresponding absolute binding free energies derived in high- and low-dielectric environment will provide a better understanding of recognition of these DNA/RNA modifications by their readers, but could also assist in modulating the activity of such readers in different applied contexts.

Data availability

The datasets used and/or analyzed during the current study are available from the corresponding author on reasonable request.

Received: 2 June 2022; Accepted: 2 November 2022

Published online: 15 November 2022

References

1. Jaenisch, R. & Bird, A. Epigenetic regulation of gene expression: How the genome integrates intrinsic and environmental signals. *Nat. Genet.* **33**, 245–254. <https://doi.org/10.1038/ng1089> (2003).
2. Chen, K., Zhao, B. S. & He, C. Nucleic acid modifications in regulation of gene expression. *Cell Chem. Biol.* **23**, 74–85. <https://doi.org/10.1016/j.chembiol.2015.11.007> (2016).
3. Shi, H., Wei, J. & He, C. Where, when, and how: Context-dependent functions of RNA methylation writers, readers, and erasers. *Mol. Cell* **74**, 640–650. <https://doi.org/10.1016/j.molcel.2019.04.025> (2019).

4. Jones, P. A. Functions of DNA methylation: Islands, start sites, gene bodies and beyond. *Nat. Rev. Genet.* **13**, 484–492. <https://doi.org/10.1038/nrg3230> (2012).
5. Breiling, A. & Lyko, F. Epigenetic regulatory functions of DNA modifications: 5-methylcytosine and beyond. *Epigenet. Chromatin* **8**, 24. <https://doi.org/10.1186/s13072-015-0016-6> (2015).
6. Rausch, C., Hastert, F. D. & Cardoso, M. C. DNA modification readers and writers and their interplay. *J. Mol. Biol.* <https://doi.org/10.1016/j.jmb.2019.12.018> (2019).
7. Roundtree, I. A. & He, C. RNA epigenetics—Chemical messages for posttranscriptional gene regulation. *Curr. Opin. Chem. Biol.* **30**, 46–51. <https://doi.org/10.1016/j.cbpa.2015.10.024> (2016).
8. Wang, X. *et al.* N6-methyladenosine-dependent regulation of messenger RNA stability. *Nature* **505**, 117–120. <https://doi.org/10.1038/nature12730> (2014).
9. Boccaletto, P. *et al.* MODOMICS: A database of RNA modification pathways. 2017 update. *Nucleic Acids Res.* **46**, D303–D307. <https://doi.org/10.1093/nar/gkx1030> (2018).
10. Boo, S. H. & Kim, Y. K. The emerging role of RNA modifications in the regulation of mRNA stability. *Exp. Mol. Med.* **52**, 400–408. <https://doi.org/10.1038/s12276-020-0407-z> (2020).
11. Zagrovic, B., Bartonek, L. & Polyansky, A. A. RNA–protein interactions in an unstructured context. *FEBS Lett.* **592**, 2901–2916. <https://doi.org/10.1002/1873-3468.13116> (2018).
12. de Ruiter, A. & Zagrovic, B. Absolute binding-free energies between standard RNA/DNA nucleobases and amino-acid sidechain analogs in different environments. *Nucleic Acids Res.* **43**, 708–718. <https://doi.org/10.1093/nar/gku1344> (2015).
13. Polyansky, A. A. & Zagrovic, B. Evidence of direct complementary interactions between messenger RNAs and their cognate proteins. *Nucleic Acids Res.* **41**, 8434–8443. <https://doi.org/10.1093/nar/gkt618> (2013).
14. Andrews, C. T., Campbell, B. A. & Elcock, A. H. Direct comparison of amino acid and salt interactions with double-stranded and single-stranded DNA from explicit-solvent molecular dynamics simulations. *J. Chem. Theory Comput.* **13**, 1794–1811. <https://doi.org/10.1021/acs.jctc.6b00883> (2017).
15. Biot, C., Buisine, E. & Rooman, M. Free-energy calculations of protein–ligand cation- π and amino- π interactions: From vacuum to protein like environments. *J. Am. Chem. Soc.* **125**, 13988–13994. <https://doi.org/10.1021/ja035223e> (2003).
16. Tuszynska, I. & Bujnicki, J. M. DARS-RNP and QUASI-RNP: New statistical potentials for protein–RNA docking. *BMC Bioinform.* **12**, 348. <https://doi.org/10.1186/1471-2105-12-348> (2011).
17. Jakubec, D., Hostas, J., Laskowski, R. A., Hobza, P. & Vondrasek, J. Large-scale quantitative assessment of binding preferences in protein–nucleic acid complexes. *J. Chem. Theory Comput.* **11**, 1939–1948. <https://doi.org/10.1021/ct501168n> (2015).
18. Akinrimisi, E. O. & Tso, P. O. Interactions of purine with proteins and amino acids. *Biochemistry* **3**, 619–626. <https://doi.org/10.1021/bi00893a004> (1964).
19. Thomas, P. D. & Podder, S. K. Specificity in protein–nucleic acid interaction: Solubility study on amino acid–nucleoside interaction. *FEBS Lett.* **96**, 90–94. [https://doi.org/10.1016/0014-5793\(78\)81069-2](https://doi.org/10.1016/0014-5793(78)81069-2) (1978).
20. Woese, C. R. Evolution of the genetic code. *Naturwissenschaften* **60**, 447–459 (1973).
21. Bie, L. H., Fei, J. W. & Gao, J. Molecular mechanism of methyl-dependent and spatial-specific DNA recognition of c-Jun homodimer. *J. Mol. Model* **27**, 227. <https://doi.org/10.1007/s00894-021-04840-y> (2021).
22. Bie, L., Du, L., Yuan, Q. & Gao, J. How a single 5-methylation of cytosine regulates the recognition of C/EBP β transcription factor: A molecular dynamic simulation study. *J. Mol. Model* **24**, 159. <https://doi.org/10.1007/s00894-018-3678-8> (2018).
23. Stephens, D. C. & Poon, G. M. Differential sensitivity to methylated DNA by ETS-family transcription factors is intrinsically encoded in their DNA-binding domains. *Nucleic Acids Res.* **44**, 8671–8681. <https://doi.org/10.1093/nar/gkw528> (2016).
24. Li, Y. *et al.* Atomistic and thermodynamic analysis of N6-methyladenosine (m(6)A) recognition by the reader domain of YTHDC1. *J. Chem. Theory Comput.* **17**, 1240–1249. <https://doi.org/10.1021/acs.jctc.0c01136> (2021).
25. Chen, X. *et al.* 5-methylcytosine promotes pathogenesis of bladder cancer through stabilizing mRNAs. *Nat. Cell Biol.* **21**, 978–990. <https://doi.org/10.1038/s41556-019-0361-y> (2019).
26. Squires, J. E. *et al.* Widespread occurrence of 5-methylcytosine in human coding and non-coding RNA. *Nucleic Acids Res.* **40**, 5023–5033. <https://doi.org/10.1093/nar/gks144> (2012).
27. Yang, X. *et al.* 5-methylcytosine promotes mRNA export—NSUN2 as the methyltransferase and ALYREF as an m5C reader. *Cell Res.* **27**, 606–625. <https://doi.org/10.1038/cr.2017.55> (2017).
28. Bachman, M. *et al.* 5-Hydroxymethylcytosine is a predominantly stable DNA modification. *Nat. Chem.* **6**, 1049–1055. <https://doi.org/10.1038/nchem.2064> (2014).
29. Delatte, B. *et al.* Transcriptome-wide distribution and function of RNA hydroxymethylcytosine. *Science* **351**, 282–285. <https://doi.org/10.1126/science.aac5253> (2016).
30. Lan, J. *et al.* Functional role of Tet-mediated RNA hydroxymethylcytosine in mouse ES cells and during differentiation. *Nat. Commun.* **11**, 4956. <https://doi.org/10.1038/s41467-020-18729-6> (2020).
31. Tahiliani, M. *et al.* Conversion of 5-methylcytosine to 5-hydroxymethylcytosine in mammalian DNA by MLL partner TET1. *Science* **324**, 930–935. <https://doi.org/10.1126/science.1170116> (2009).
32. Greer, E. L. *et al.* DNA methylation on N6-adenine in *C. elegans*. *Cell* **161**, 868–878. <https://doi.org/10.1016/j.cell.2015.04.005> (2015).
33. Wu, T. P. *et al.* DNA methylation on N6-adenine in mammalian embryonic stem cells. *Nature* **532**, 329–333. <https://doi.org/10.1038/nature17640> (2016).
34. Zhang, G. *et al.* N6-Methyladenine DNA modification in *Drosophila*. *Cell* **161**, 893–906. <https://doi.org/10.1016/j.cell.2015.04.018> (2015).
35. Yang, C. *et al.* The role of m6A modification in physiology and disease. *Cell Death Dis.* **11**, 960. <https://doi.org/10.1038/s41419-020-03143-z> (2020).
36. Goll, M. G. & Bestor, T. H. Eukaryotic cytosine methyltransferases. *Annu. Rev. Biochem.* **74**, 481–514. <https://doi.org/10.1146/annurev.biochem.74.010904.153721> (2005).
37. Kumar, S., Chinnusamy, V. & Mohapatra, T. Epigenetics of modified DNA bases: 5-methylcytosine and beyond. *Front. Genet.* **9**, 640. <https://doi.org/10.3389/fgene.2018.00640> (2018).
38. Klose, R. J. & Bird, A. P. Genomic DNA methylation: The mark and its mediators. *Trends Biochem. Sci.* **31**, 89–97. <https://doi.org/10.1016/j.tibs.2005.12.008> (2006).
39. Nan, X. *et al.* Transcriptional repression by the methyl-CpG-binding protein MeCP2 involves a histone deacetylase complex. *Nature* **393**, 386–389. <https://doi.org/10.1038/30764> (1998).
40. Ng, H.-H. *et al.* MBD2 is a transcriptional repressor belonging to the MeCP1 histone deacetylase complex. *Nat. Genet.* **23**, 58–61. <https://doi.org/10.1038/12659> (1999).
41. Schübeler, D. Function and information content of DNA methylation. *Nature* **517**, 321–326. <https://doi.org/10.1038/nature14192> (2015).
42. Domcke, S. *et al.* Competition between DNA methylation and transcription factors determines binding of NRF1. *Nature* **528**, 575–579. <https://doi.org/10.1038/nature16462> (2015).
43. Ito, S. *et al.* Role of Tet proteins in 5mC to 5hmC conversion, ES-cell self-renewal and inner cell mass specification. *Nature* **466**, 1129–1133. <https://doi.org/10.1038/nature09303> (2010).

44. Kriaucionis, S. & Heintz, N. The nuclear DNA base 5-hydroxymethylcytosine is present in Purkinje neurons and the brain. *Science* **324**, 929–930. <https://doi.org/10.1126/science.1169786> (2009).
45. Delatte, B. *et al.* RNA biochemistry. Transcriptome-wide distribution and function of RNA hydroxymethylcytosine. *Science* **351**, 282–285. <https://doi.org/10.1126/science.aac5253> (2016).
46. Zaccara, S., Ries, R. J. & Jaffrey, S. R. Reading, writing and erasing mRNA methylation. *Nat. Rev. Mol. Cell Biol.* **20**, 608–624. <https://doi.org/10.1038/s41580-019-0168-5> (2019).
47. Zhen, D. *et al.* m(6)A reader: Epitranscriptome target prediction and functional characterization of N(6)-methyladenosine (m(6)A) readers. *Front. Cell Dev. Biol.* **8**, 741. <https://doi.org/10.3389/fcell.2020.00741> (2020).
48. Fu, Y. *et al.* N6-Methyldeoxyadenosine marks active transcription start sites in *Chlamydomonas*. *Cell* **161**, 879–892. <https://doi.org/10.1016/j.cell.2015.04.010> (2015).
49. Zhu, W. *et al.* Detection of N6-methyladenosine modification residues (review). *Int. J. Mol. Med.* <https://doi.org/10.3892/ijmm.2019.4169> (2019).
50. Alseth, I., Dalhus, B. & Bjørås, M. Inosine in DNA and RNA. *Curr. Opin. Genet. Dev.* **26**, 116–123. <https://doi.org/10.1016/j.gde.2014.07.008> (2014).
51. Mozgova, I. & Köhler, C. DNA-sequence-specific erasers of epigenetic memory. *Nat. Genet.* **48**, 591–592. <https://doi.org/10.1038/ng.3579> (2016).
52. Li, L., Li, C., Zhang, Z. & Alexov, E. On the dielectric “constant” of proteins: Smooth dielectric function for macromolecular modeling and its implementation in DelPhi. *J. Chem. Theory Comput.* **9**, 2126–2136. <https://doi.org/10.1021/ct400065j> (2013).
53. Hajnic, M., Ruiter, A. D., Polyansky, A. A. & Zagrovic, B. Inosine nucleobase acts as guanine in interactions with protein side chains. *J. Am. Chem. Soc.* **138**, 5519–5522. <https://doi.org/10.1021/jacs.6b02417> (2016).
54. de Ruiter, A., Polyansky, A. A. & Zagrovic, B. Dependence of binding free energies between RNA nucleobases and protein side chains on local dielectric properties. *J. Chem. Theory Comput.* **13**, 4504–4513. <https://doi.org/10.1021/acs.jctc.6b01202> (2017).
55. Oostenbrink, C., Villa, A., Mark, A. E. & Van Gunsteren, W. F. A biomolecular force field based on the free enthalpy of hydration and solvation: The GROMOS force-field parameter sets 53A5 and 53A6. *J. Comput. Chem.* **25**, 1656–1676. <https://doi.org/10.1002/jcc.20090> (2004).
56. Pronk, S. *et al.* GROMACS 4.5: A high-throughput and highly parallel open source molecular simulation toolkit. *Bioinformatics* **29**, 845–854. <https://doi.org/10.1093/bioinformatics/btt055> (2013).
57. Abraham, M. J. *et al.* GROMACS: High performance molecular simulations through multi-level parallelism from laptops to supercomputers. *SoftwareX* **1–2**, 19–25 (2015).
58. Berendsen, H. J. C., Postma, J. P. M., van Gunsteren, W. F., DiNola, A. & Haak, J. R. Molecular dynamics with coupling to an external bath. *J. Chem. Phys.* **81**, 3684–3690. <https://doi.org/10.1063/1.448118> (1984).
59. Heinz, T. N., van Gunsteren, W. F. & Hünenberger, P. H. Comparison of four methods to compute the dielectric permittivity of liquids from molecular dynamics simulations. *J. Chem. Phys.* **115**, 1125–1136. <https://doi.org/10.1063/1.1379764> (2001).
60. Hess, B., Bekker, H., Berendsen, H. J. C. & Fraaije, J. G. E. M. LINCS: A linear constraint solver for molecular simulations. *J. Comput. Chem.* **18**, 1463–1472. [https://doi.org/10.1002/\(SICI\)1096-987X\(199709\)18:12%3c1463::AID-JCC4%3e3.0.CO;2-H](https://doi.org/10.1002/(SICI)1096-987X(199709)18:12%3c1463::AID-JCC4%3e3.0.CO;2-H) (1997).
61. Walser, R., Mark, A. E., van Gunsteren, W. F., Lauterbach, M. & Wipff, G. The effect of force-field parameters on properties of liquids: Parametrization of a simple three-site model for methanol. *J. Chem. Phys.* **112**, 10450–10459. <https://doi.org/10.1063/1.481680> (2000).
62. Haynes, W. M. *CRC Handbook of Chemistry and Physics* 94th edn. (CRC Press, 2013).
63. Caleman, C. *et al.* Force field benchmark of organic liquids: Density, enthalpy of vaporization, heat capacities, surface tension, isothermal compressibility, volumetric expansion coefficient, and dielectric constant. *J. Chem. Theory Comput.* **8**, 61–74. <https://doi.org/10.1021/ct200731v> (2012).
64. Marcus, Y. *The Properties of Solvents* (Wiley, 1998).
65. Atchley, W. R., Zhao, J., Fernandes, A. D. & Druke, T. Solving the protein sequence metric problem. *Proc. Natl. Acad. Sci. USA* **102**, 6395–6400. <https://doi.org/10.1073/pnas.0408677102> (2005).
66. Yang, J. *et al.* Structural basis for effects of CpA modifications on C/EBP β binding of DNA. *Nucleic Acids Res.* **47**, 1774–1785. <https://doi.org/10.1093/nar/gky1264> (2019).
67. Miller, M. The importance of being flexible: The case of basic region leucine zipper transcriptional regulators. *Curr. Protein Pept. Sci.* **10**, 244–269. <https://doi.org/10.2174/138920309788452164> (2009).
68. Ngo, T. T. M. *et al.* Effects of cytosine modifications on DNA flexibility and nucleosome mechanical stability. *Nat. Commun.* **7**, 10813. <https://doi.org/10.1038/ncomms10813> (2016).
69. Engel, J. D. & von Hippel, P. H. Effects of methylation on the stability of nucleic acid conformations. Studies at the polymer level. *J. Biol. Chem.* **253**, 927–934 (1978).
70. Mierzejewska, K. *et al.* Structural basis of the methylation specificity of R.DpnI. *Nucleic Acids Res.* **42**, 8745–8754. <https://doi.org/10.1093/nar/gku546> (2014).
71. Bochtler, M. & Fernandes, H. DNA adenine methylation in eukaryotes: Enzymatic mark or a form of DNA damage?. *BioEssays* **43**, e2000243. <https://doi.org/10.1002/bies.202000243> (2021).
72. Liu, N. *et al.* N6-methyladenosine-dependent RNA structural switches regulate RNA–protein interactions. *Nature* **518**, 560–564. <https://doi.org/10.1038/nature14234> (2015).
73. Chakravorty, A. *et al.* Gaussian-based smooth dielectric function: A surface-free approach for modeling macromolecular binding in solvents. *Front. Mol. Biosci.* **5**, 25. <https://doi.org/10.3389/fmolb.2018.00025> (2018).
74. Jolma, A. *et al.* DNA-binding specificities of human transcription factors. *Cell* **152**, 327–339. <https://doi.org/10.1016/j.cell.2012.12.009> (2013).
75. Rohs, R. *et al.* The role of DNA shape in protein–DNA recognition. *Nature* **461**, 1248–1253. <https://doi.org/10.1038/nature08473> (2009).
76. Siggers, T., Duyzend, M. H., Reddy, J., Khan, S. & Bulyk, M. L. Non-DNA-binding cofactors enhance DNA-binding specificity of a transcriptional regulatory complex. *Mol. Syst. Biol.* **7**, 555. <https://doi.org/10.1038/msb.2011.89> (2011).
77. Bai, L. & Morozov, A. V. Gene regulation by nucleosome positioning. *Trends Genet.* **26**, 476–483. <https://doi.org/10.1016/j.tig.2010.08.003> (2010).

Acknowledgements

The authors gratefully acknowledge Prof. C. Oostenbrink for help with parameterization of modified nucleobases.

Author contributions

M.H., A.R., and B.Z. designed research; M.H., S.A.G., A.A.P. and A.R. carried out research; M.H., S.A.G. and B.Z. prepared figures; M.H., and B.Z. wrote the main manuscript text with input from all authors. All authors reviewed the manuscript.

Funding

This work was supported by the European Research Council Starting Independent grant 279408 and the Volkswagenstiftung LIFE grant to BZ, and the European Union's Framework Programme for Research and Innovation Horizon 2020 (2014-2020) under the Marie Curie Skłodowska Grant Agreement Nr. 847548.

Competing interests

The authors declare no competing interests.

Additional information

Supplementary Information The online version contains supplementary material available at <https://doi.org/10.1038/s41598-022-23585-z>.

Correspondence and requests for materials should be addressed to B.Z.

Reprints and permissions information is available at www.nature.com/reprints.

Publisher's note Springer Nature remains neutral with regard to jurisdictional claims in published maps and institutional affiliations.



Open Access This article is licensed under a Creative Commons Attribution 4.0 International License, which permits use, sharing, adaptation, distribution and reproduction in any medium or format, as long as you give appropriate credit to the original author(s) and the source, provide a link to the Creative Commons licence, and indicate if changes were made. The images or other third party material in this article are included in the article's Creative Commons licence, unless indicated otherwise in a credit line to the material. If material is not included in the article's Creative Commons licence and your intended use is not permitted by statutory regulation or exceeds the permitted use, you will need to obtain permission directly from the copyright holder. To view a copy of this licence, visit <http://creativecommons.org/licenses/by/4.0/>.

© The Author(s) 2022